Calcium signaling in the photodamaged skin: *in vivo* experiments and mathematical modeling

Authors

Viola Donati[1,2,†], Chiara Peres[2,†], Chiara Nardin[2], Ferdinando Scavizzi[2], Marcello Raspa[2], Catalin D. Ciubotaru[3], Mario Bortolozzi[1,2,4,*], Morten Gram Pedersen[5,6,*], and Fabio Mammano[1,2,**]

Affiliations

[1]Department of Physics and Astronomy "G. Galilei", University of Padova, 35131 Padova, Italy.
[2]CNR Institute of Biochemistry and Cell Biology, 00015 Monterotondo (RM), Italy.
[3]CNR IOM Materials Foundry, 34149 Basovizza (TS), Italy.
[4]Veneto Institute of Molecular Medicine (VIMM), 35129 Padova (PD), Italy.
[5]Department of Information Engineering, University of Padova, 35131 Padova (PD), Italy.
[6]Department of Mathematics "Tullio Levi-Civita", University of Padova, 35121 Padova (PD), Italy.
† Equal contribution.
* Corresponding authors: mortengram.pedersen@unipd.it, mario.bortolozzi@unipd.it
**Corresponding author and lead contact: fabio.mammano@unipd.it

Supplementary materials

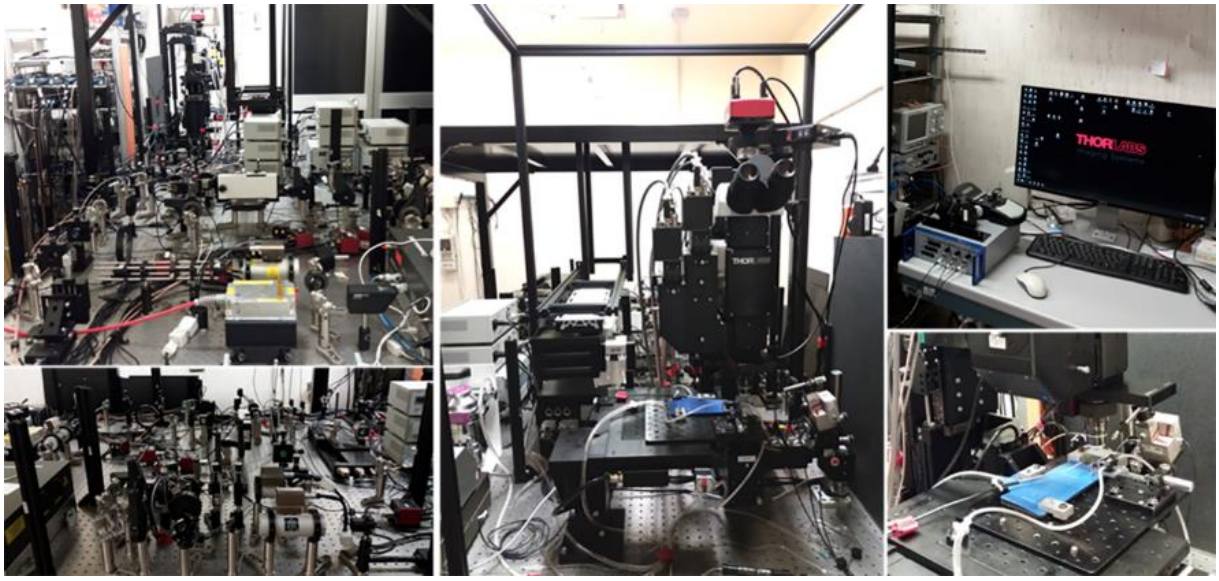

Figure S1: Photograph of the multiphoton-STED intravital microscopy facility at CNR, Rome.

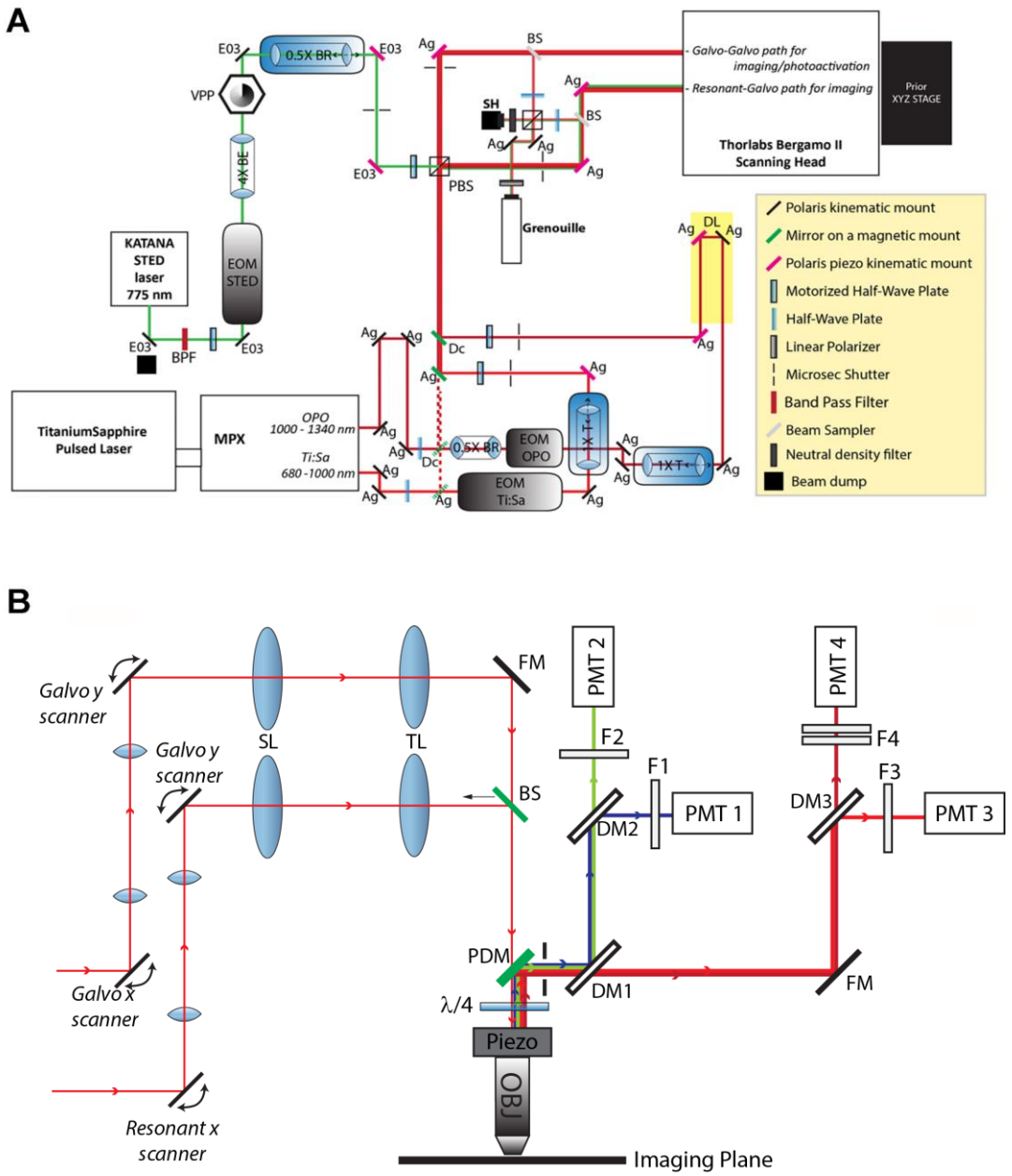

Figure S2: Simplified optical scheme of the optical paths and multiphoton microscope. (**A**) Optical bench optics used to deliver 3 laser lines to the two scanning heads of the multiphoton microscope. VPP, vortex phase plate; SH, Shack-Hartmann wavefront sensor; Grenouille, beam profiler; Ag, silver-coated mirrors; Dc, dichroic mirror; E03, dielectric mirrors; PBS, polarizing beam splitter; EOM, electro-optical modulators; BS, beam sampler; BE, beam expander; BR, beam reducer; T, variable telescope used to control beam divergence. DL, optical delay line, used to synchronize PUMP and OPO pulses. (**B**) Multiphoton microscope. Red lines entering from the left represent titanium-sapphire (Ti:Sa) laser beams impinging on the pair of scanning systems. SL: Scan Lens; TL: Tube Lens; FM: Full Mirror; BS: 50/50 Beam splitter; PDM: Primary Dichroic Mirror; λ/4: Quarter wave plate; Piezo: Piezo Objective Scanner; Obj: Objective lens; DM1: 565 nm long pass filter (T565lpxr); DM2: 495 nm long pass filter (T495lpxru); DM3: 652 long pass filter (FF652- Di01-25x36); F1: 460/50 nm band pass filter (ET460/50m-2p); F2: 525/40 nm band pass filter (FF02-525/40-25); F3: 612/69 band pass filter (FF01-612/69-25); F4: combination of 647 nm long pass filter (BLP01-647R-25) and 770 nm short pass filter (FF01-770/SP-25); NF: Notch Filter; PMT: photomultiplier tube; PDT: photodiode tube.

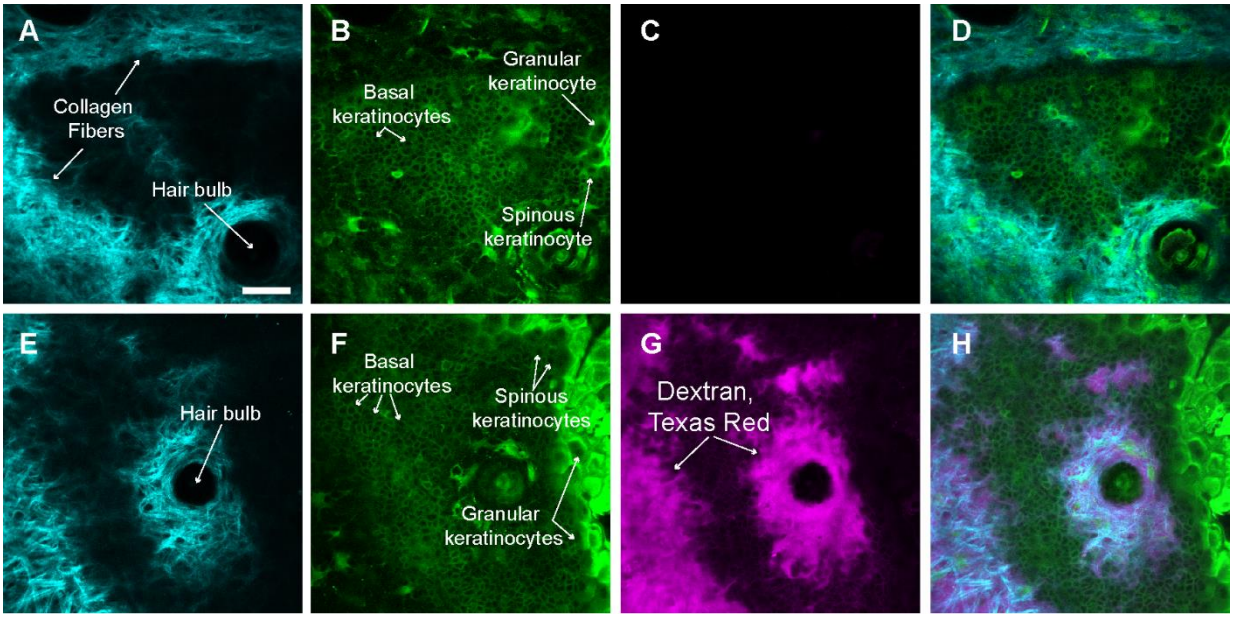

Figure S3: Images acquired in two different fields of view (FOVs) with different emission channels of the multiphoton microscope while exciting the mouse epidermis *in vivo* at 920 nm before (**A-D**, FOV #1) and after (**E-H**, FOV #2) injection of a high molecular weight (70 kDa) dextran molecule conjugated with a red fluorescent dye (Texas Red). (**A, E**) Second harmonic generation (SHG) allows the imaging of collagen fibers, represented in cyan color. (**B, F**) GCaMP6s and keratinocytes autofluorescence are shown in green color. (**C**, **G**) Red emission channel before and after injection of red fluorescent dextran, respectively. (**D, H**) Composite images of the three channels. Arrows indicate salient features of the epidermal layers under investigation. Basal keratinocytes are the smaller polygonal green cells in the large flat area where collagen fibers are not present; larger polygonal cells are keratinocytes of the spinous and granular epidermal layers. Oval-shaped hollows, surrounded by collagen fibers in **A** and **E** correspond to hair bulbs and related appendages, such as sebaceous glands. Scale bar: 50 µm.

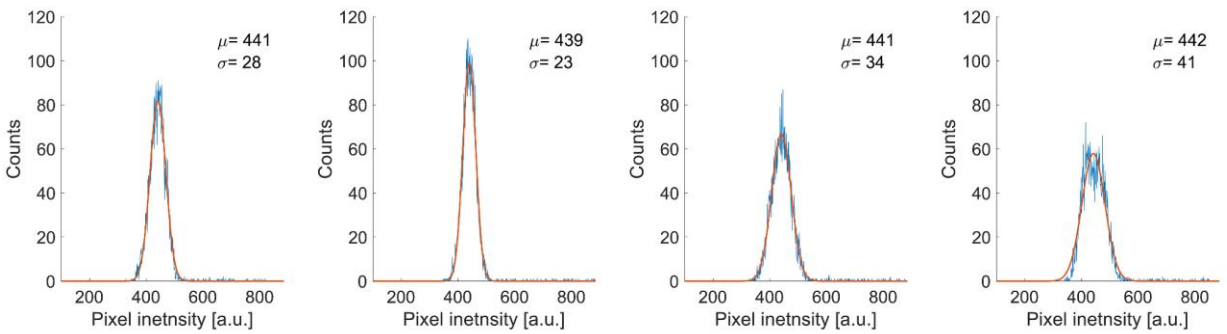

Figure S4: Histograms of the pixel intensity (blue traces) in ROIs composed of 76 x 76 pixels within an image region where the keratinocytes were present. G_1 fitting curves (orange traces) are shown together with the corresponding fitting paramaters, μ_1 and σ_1.

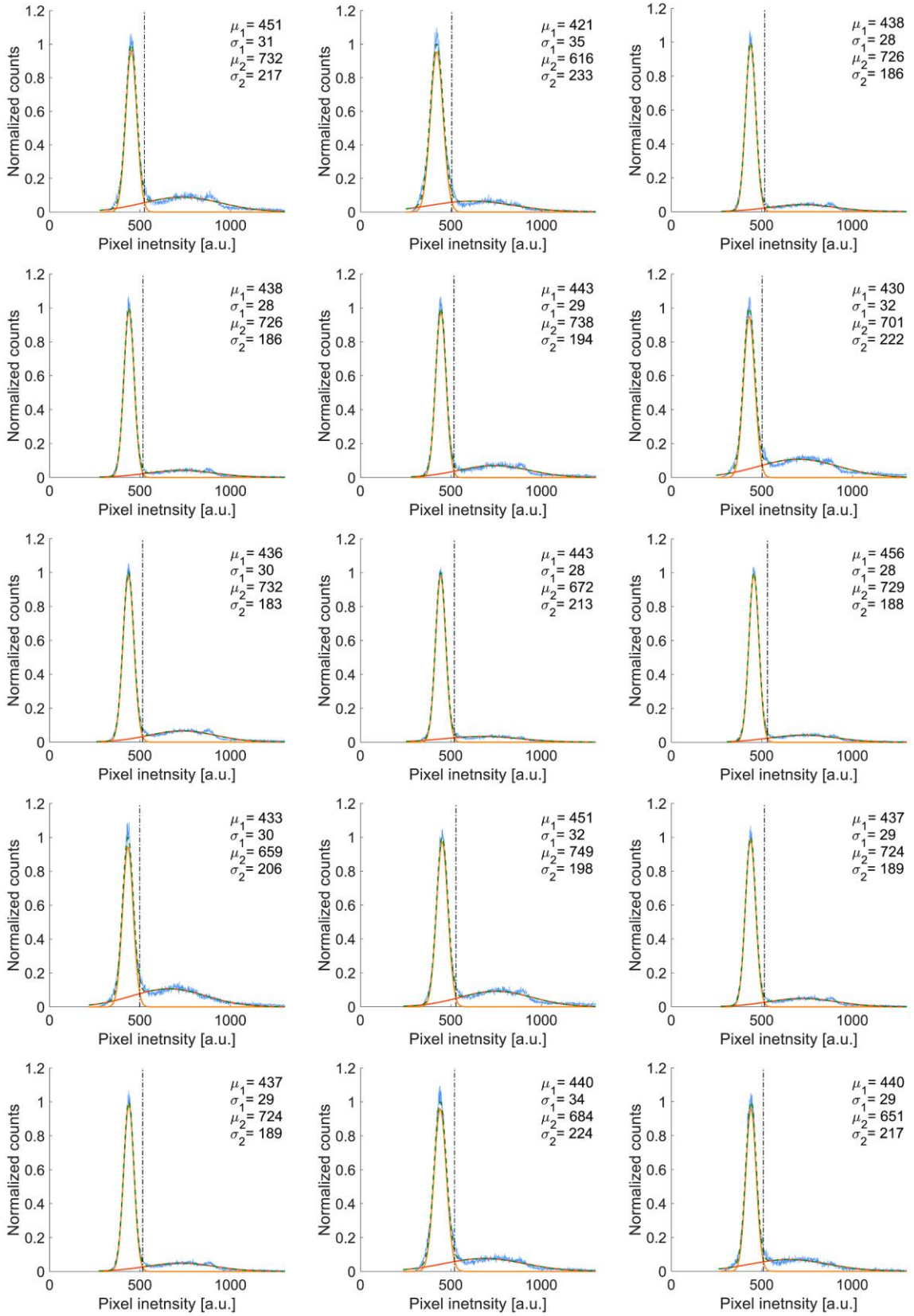

Figure S5: Background Subtraction. Shown are histograms of the pixel intensity (normalized to the maximum of the first peak) in a ROI of 76x76 pixels taken in a region where the keratinocytes were present in the first 5 frames before the photodamage. Each histogram corresponds to n ≥ 3 videos in m = 1 u-GCaMP6s mouse (blue) and the double Gaussian fit (green dashed line) is shown together with the μ and σ of each Gaussian distribution. The intersection between the two fitting distributions (yellow and orange), marked by a vertical dash-dotted line, was used for background subtraction (see text).

Vehicle solution

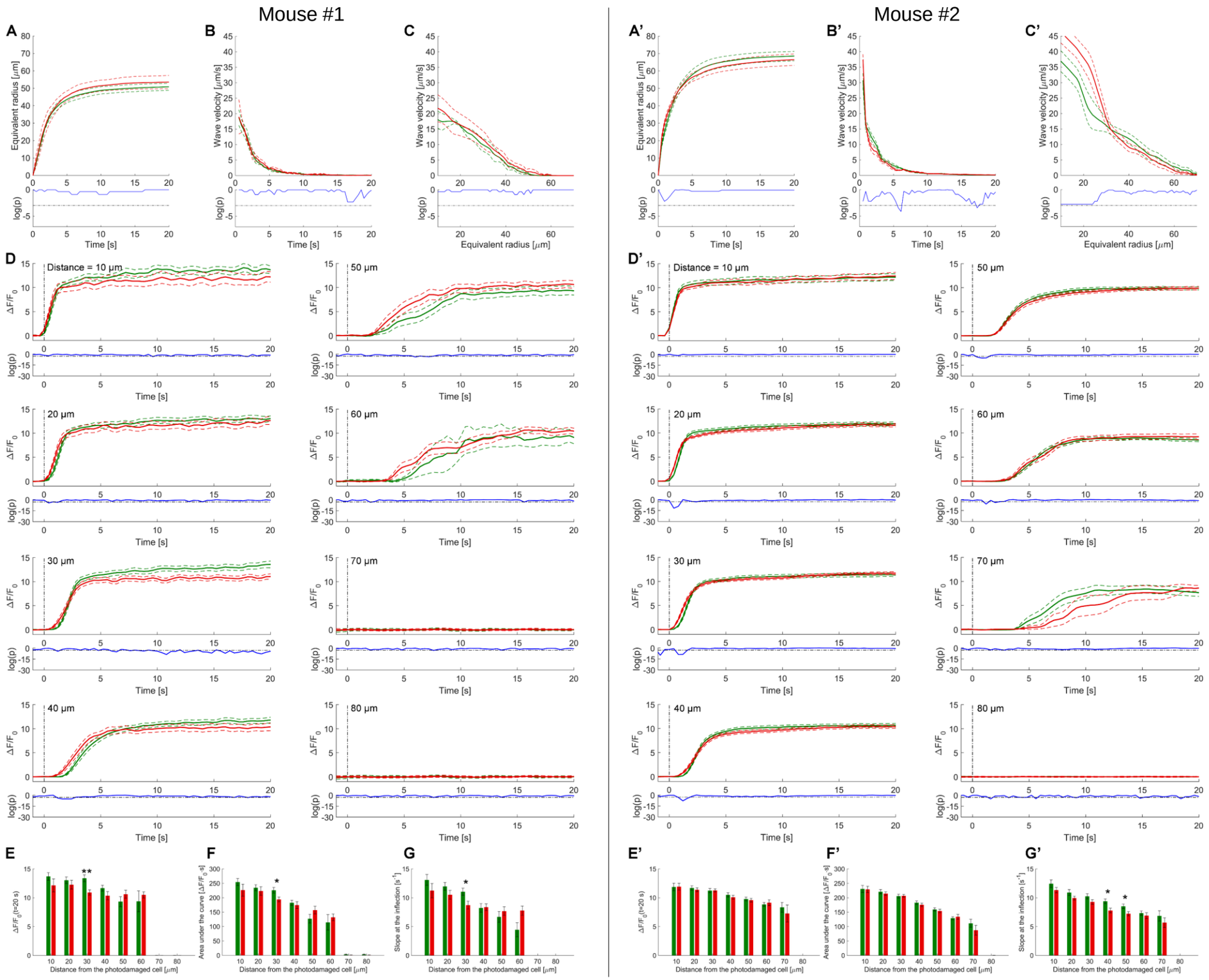

Figure S6: Effect of vehicle solution (VS) microinjection on Ca^{2+} wave expansion after focal photodamage. (**A**) Equivalent radius of the area invaded by Ca^{2+} waves as a function of time after photodamage; speed of the expanding wave as function of time (**B**) and of the equivalent radius (**C**). (**D**) $\Delta F(t)/F_0$ responses of bystander keratinocytes at increasing distance from the photodamage site. In each panel, the vertical black dash-dotted line at 0 s marks the end of the 0.5 s photodamage time interval. Data in (**A-D**) are mean (solid line) ± s.e.m. (dashed line) in control conditions (green) and after VS microinjection (red). Point-by-point p-values (p; Wilcoxon Rank Sum test for **A-C**; two-sample t-test for **D**) are shown on a logarithmic scale below each graph (blue traces); $p < 0.05$ (horizontal black dash-dotted line) indicates statistical significance. (**E**) Amplitude (a) of the $\Delta F(t)/F_0$ trace at time t=20 s. (**F**) Area (I) under the$\Delta F(t)/F_0$ trace, computed between 0 and 20 s. (**G**) Slope (s) of the $\Delta F(t)/F_0$ trace at the inflection point. Data in (**E-G**) are mean ± s.e.m. vs. bystander cell distance from the photodamage site in control conditions (green) and after VS microinjection (red). P-values differences are shown above each pair of bars (two-sample t-test): * = p-value<0.05; ** = p-value<0.005. (**A'-G'**) The same experiments were repeated on a different mouse, in n=4 (control) and n=5 (VS) non-overlapping areas of earlobe skin.

Apyrase

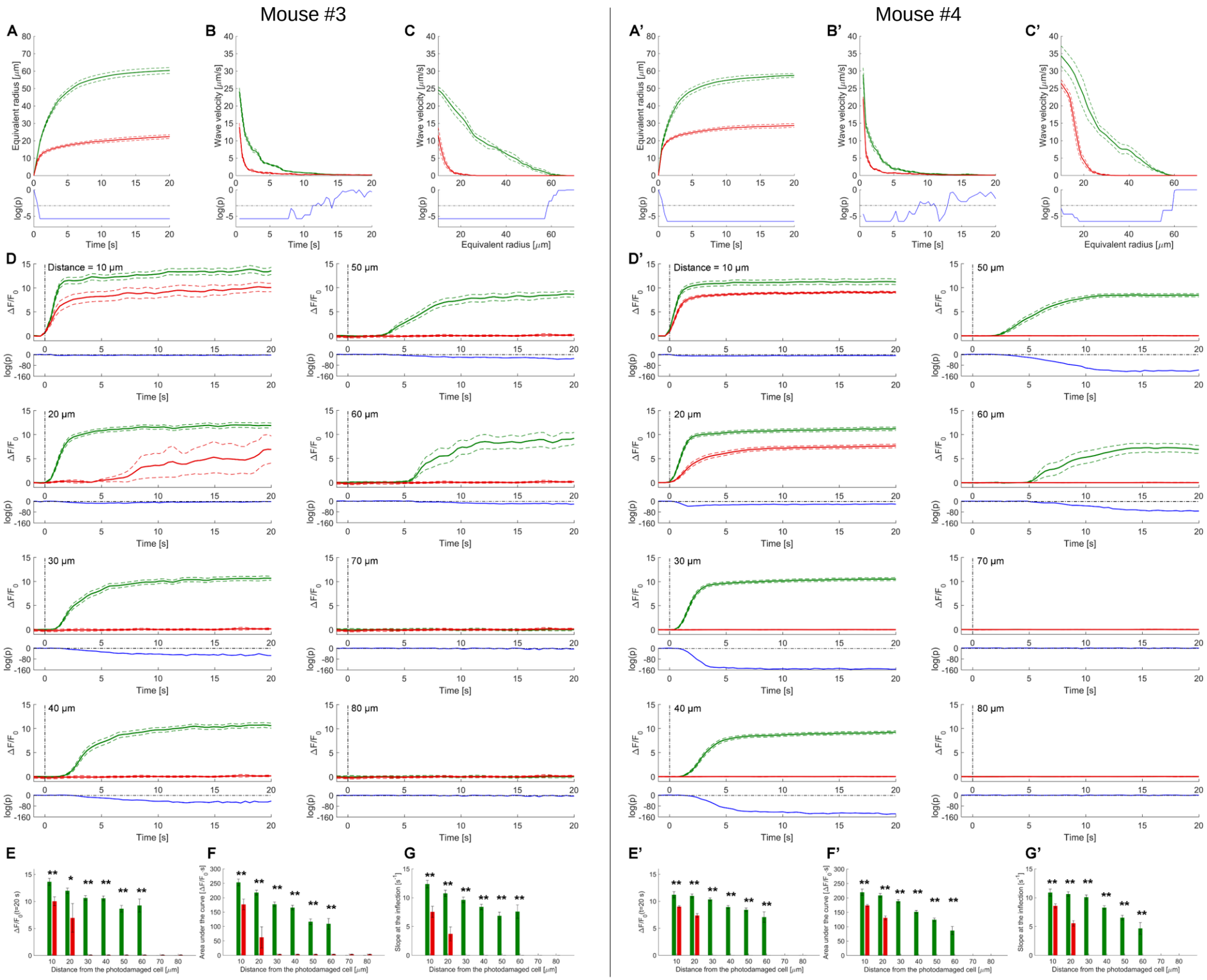

Figure S7: Effect of apyrase. (**A**) Equivalent radius of the area invaded by Ca^{2+} waves as a function of time after photodamage; speed of the expanding wave as function of time (**B**) and of the equivalent radius (**C**). (**D**) $\Delta F(t)/F_0$ responses of bystander keratinocytes at increasing distance from the photodamage site. In each panel, the vertical black dash-dotted line at 0 s marks the end of the 0.5 s photodamage time interval. Data in (**A-D**) are mean (solid line) ± s.e.m. (dashed line) in control conditions (green) and after 500 U/ml apyrase microinjection (red). Point-by-point p-values (p; Wilcoxon Rank Sum test for **A-C**; two-sample t-test for **D**) are shown on a logarithmic scale below each graph (blue traces); $p < 0.05$ (horizontal black dash-dotted line) indicates statistical significance. (**E**) Amplitude of the $\Delta F(t)/F_0$ signal at time t=20 s. (**F**) Area (I) under the$\Delta F(t)/F_0$trace, computed between 0 and 20 s. (**G**) Slope (s) of the $\Delta F(t)/F_0$ trace at the inflection point. Data in (**E-G**) are mean ± s.e.m. vs. bystander cell distance from the photodamage site in control conditions (green) and after apyrase microinjection (red). Experiments in **A-G** were conducted in n=5 (control) and n=6 (apyrase) non-overlapping areas of the mouse earlobe skin. P-values differences in **E-G** are shown above each pair of bars (two-sample t-test): *=p-value<0.05; **=p-value<0.005. (**A'-G'**) The same experiments were repeated on a different mouse, in n=5 (control) and n=7 (apyrase) non-overlapping areas of earlobe skin.

PPADS

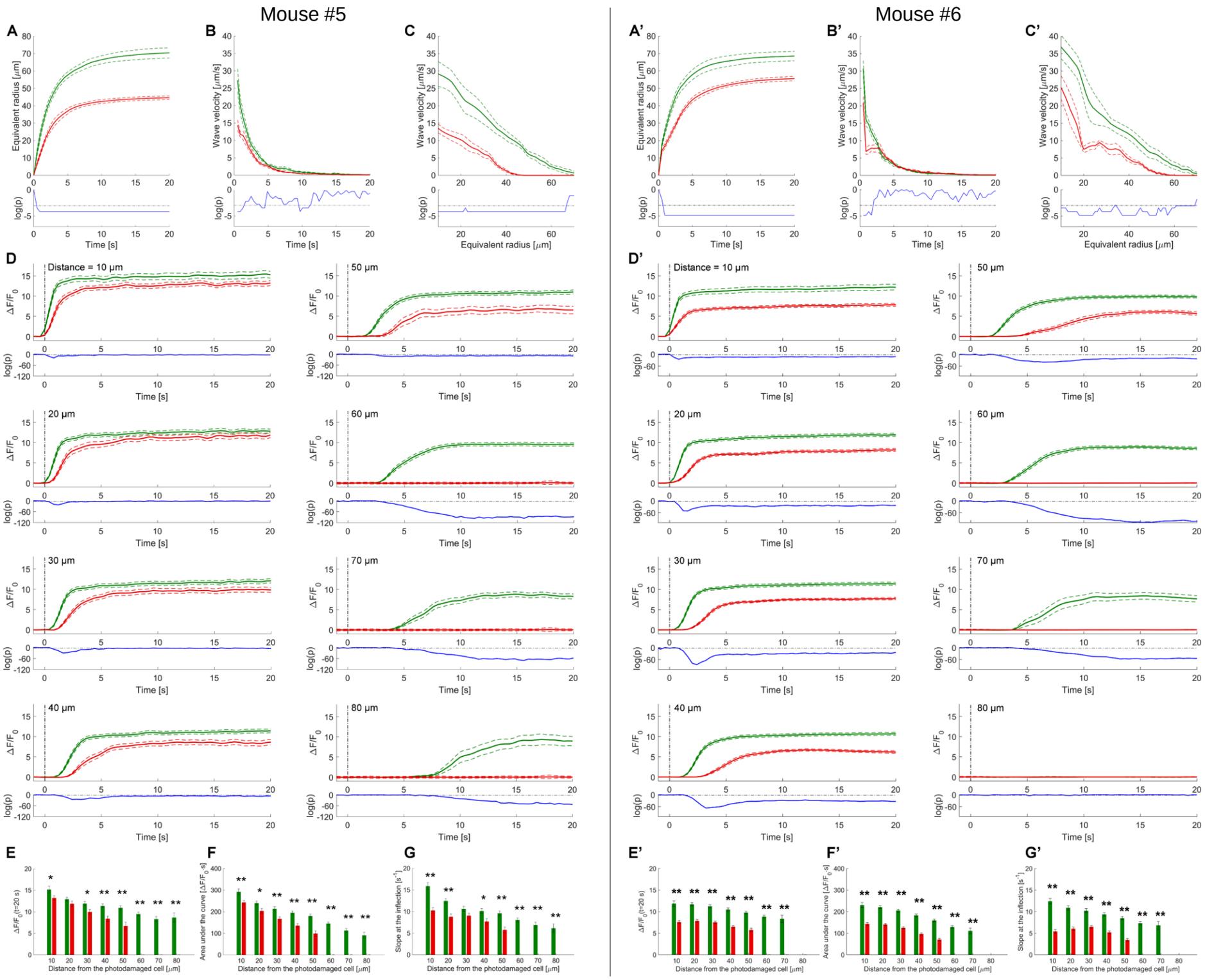

Figure S8: Effect of PPADS. (**A**) Equivalent radius of the area invaded by Ca^{2+} waves as a function of time after photodamage; speed of the expanding wave as function of time (**B**) and of the equivalent radius (**C**). (**D**) $\Delta F(t)/F_0$ responses of bystander keratinocytes at increasing distance from the photodamage site. In each panel, the vertical black dash-dotted line at 0 s marks the end of the 0.5 s photodamage time interval. Data in (**A-D**) are mean (solid line) ± s.e.m. (dashed line) in control conditions (green) and after PPADS (625 μM) microinjection (red). Point-by-point p-values (p; Wilcoxon Rank Sum test for **A-C**; two-sample t-test for **D**) are shown on a logarithmic scale below each graph (blue traces); p < 0.05 (horizontal black dash-dotted line) indicates statistical significance. (**E**) Amplitude of the $\Delta F(t)/F_0$ signal at time t=20 s. (**F**) Area (I) under the $\Delta F(t)/F_0$trace, computed between 0 and 20 s. (**G**) Slope (s) of the $\Delta F(t)/F_0$ trace at the inflection point. Data in (**E-G**) are mean ± s.e.m. vs. bystander cell distance from the photodamage site in control conditions (green) and after PPADS microinjection (red). Experiments in **A-G** were conducted in n=4 (control) and n=5 (PPADS) non-overlapping areas of the mouse earlobe skin. P-values differences in **E-G** are shown above each pair of bars (two-sample t-test): *=p-value<0.05; **=p-value<0.005. (**A'-G'**) The same experiments were repeated on a different mouse, in n=5 (control) and n=5 (PPADS) non-overlapping areas of earlobe skin.

ARL 67156

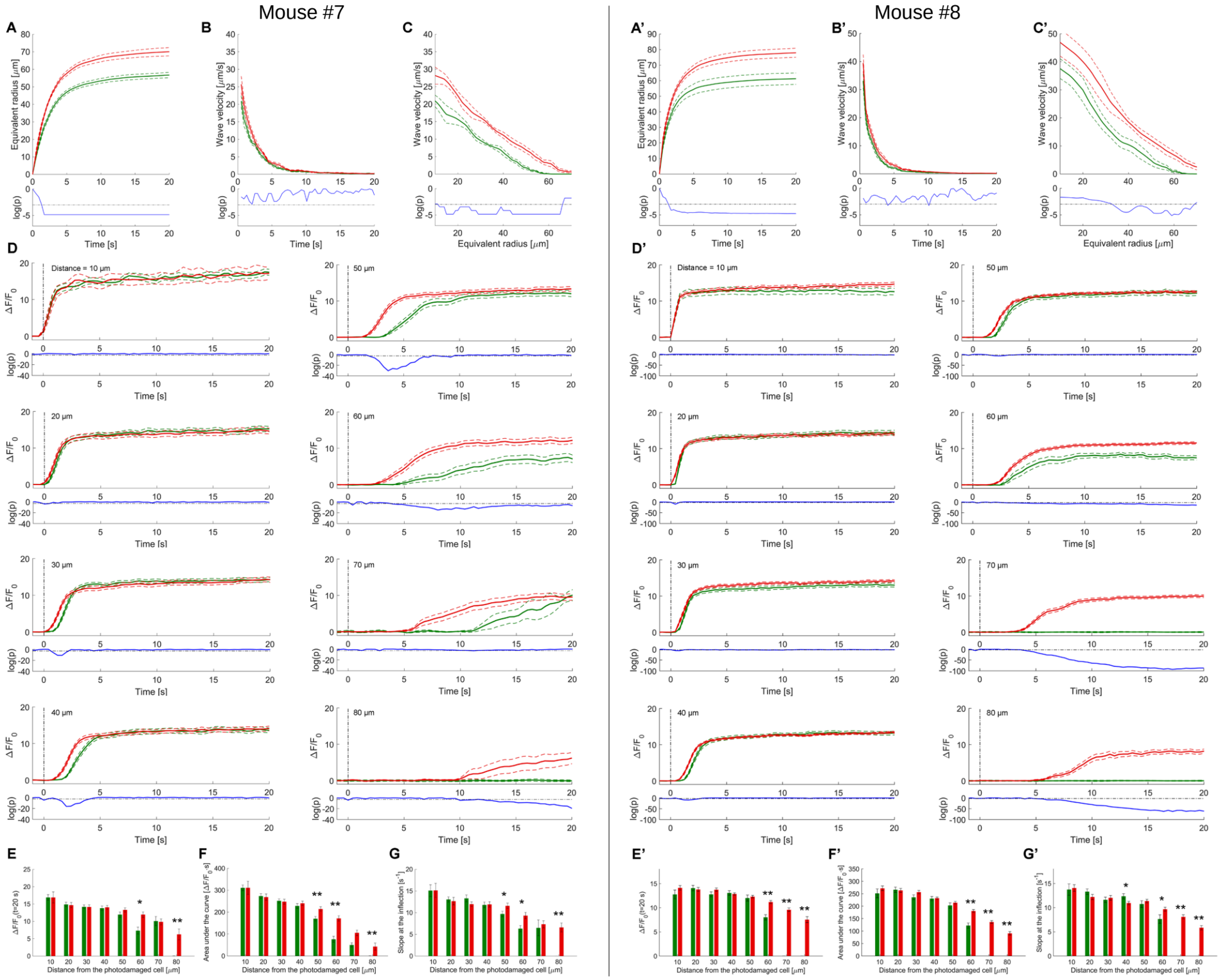

Figure S9: Effect of ARL 67156 (ARL). (**A**) Equivalent radius of the area invaded by Ca^{2+} waves as a function of time after photodamage; speed of the expanding wave as function of time (**B**) and of the equivalent radius (**C**). (**D**) $\Delta F(t)/F_0$ responses of bystander keratinocytes at increasing distance from the photodamage site. In each panel, the vertical black dash-dotted line at 0 s marks the end of the 0.5 s photodamage time interval. Data in (**A-D**) are mean (solid line) ± s.e.m. (dashed line) in control conditions (green) and after ARL (400 μM) microinjection (red). Point-by-point p-values (p; Wilcoxon Rank Sum test for **A-C**; two-sample t-test for **D**) are shown on a logarithmic scale below each graph (blue traces); $p < 0.05$ (horizontal black dash-dotted line) indicates statistical significance. (**E**) Amplitude of the $\Delta F(t)/F_0$ signal at time t=20 s. (**F**) Area (I) under the $\Delta F(t)/F_0$trace, computed between 0 and 20 s. (**G**) Slope (s) of the $\Delta F(t)/F_0$ trace at the inflection point. Data in (**E-G**) are mean ± s.e.m. vs. bystander cell distance from the photodamage site in control conditions (green) and after ARL microinjection (red). Experiments in **A-G** were conducted in n=5 (control) and n=5 (ARL) non-overlapping areas of the mouse earlobe skin. P-values differences in **E-G** are shown above each pair of bars (two-sample t-test): *=p-value<0.05; **=p-value<0.005. (**A'-G'**) The same experiments were repeated on a different mouse, in n=4 (control) and n=5 (ARL) non-overlapping areas of earlobe skin.

EGTA

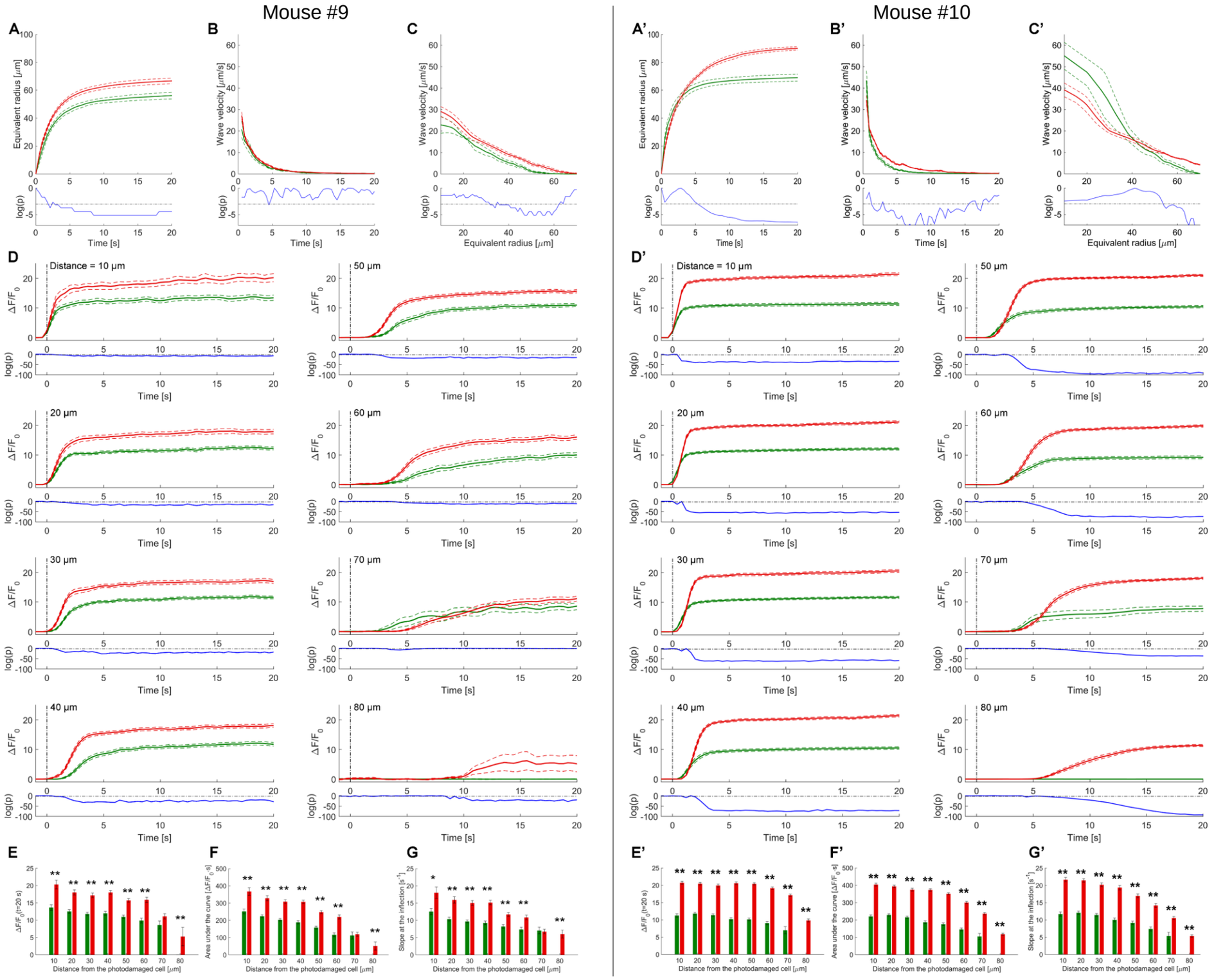

Figure S10: Effect of EGTA. (**A**) Equivalent radius of the area invaded by Ca^{2+} waves as a function of time after photodamage; speed of the expanding wave as function of time (**B**) and of the equivalent radius (**C**). (**D**) $\Delta F(t)/F_0$ responses of bystander keratinocytes at increasing distance from the photodamage site. In each panel, the vertical black dash-dotted line at 0 s marks the end of the 0.5 s photodamage time interval. Data in (**A-D**) are mean (solid line) ± s.e.m. (dashed line) in control conditions (green) and after EGTA (5 mM) microinjection (red). Point-by-point p-values (p; Wilcoxon Rank Sum test for **A-C**; two-sample t-test for **D**) are shown on a logarithmic scale below each graph (blue traces); $p < 0.05$ (horizontal black dash-dotted line) indicates statistical significance. (**E**) Amplitude of the $\Delta F(t)/F_0$ signal at time t=20 s. (**F**) Area (I) under the $\Delta F(t)/F_0$trace, computed between 0 and 20 s. (**G**) Slope (s) of the $\Delta F(t)/F_0$ trace at the inflection point. Data in (**E-G**) are mean ± s.e.m. vs. bystander cell distance from the photodamage site in control conditions (green) and after EGTA microinjection (red). Experiments in **A-G** were conducted in n=4 (control) and n=7 (EGTA) non-overlapping areas of the mouse earlobe skin. P-values differences in **E-G** are shown above each pair of bars (two-sample t-test): *=p-value<0.05; **=p-value<0.005. (**A'-G'**) The same experiments were repeated on a different mouse, in n=3 (control) and n=3 (EGTA) non-overlapping areas of earlobe skin.

Thapsigargin

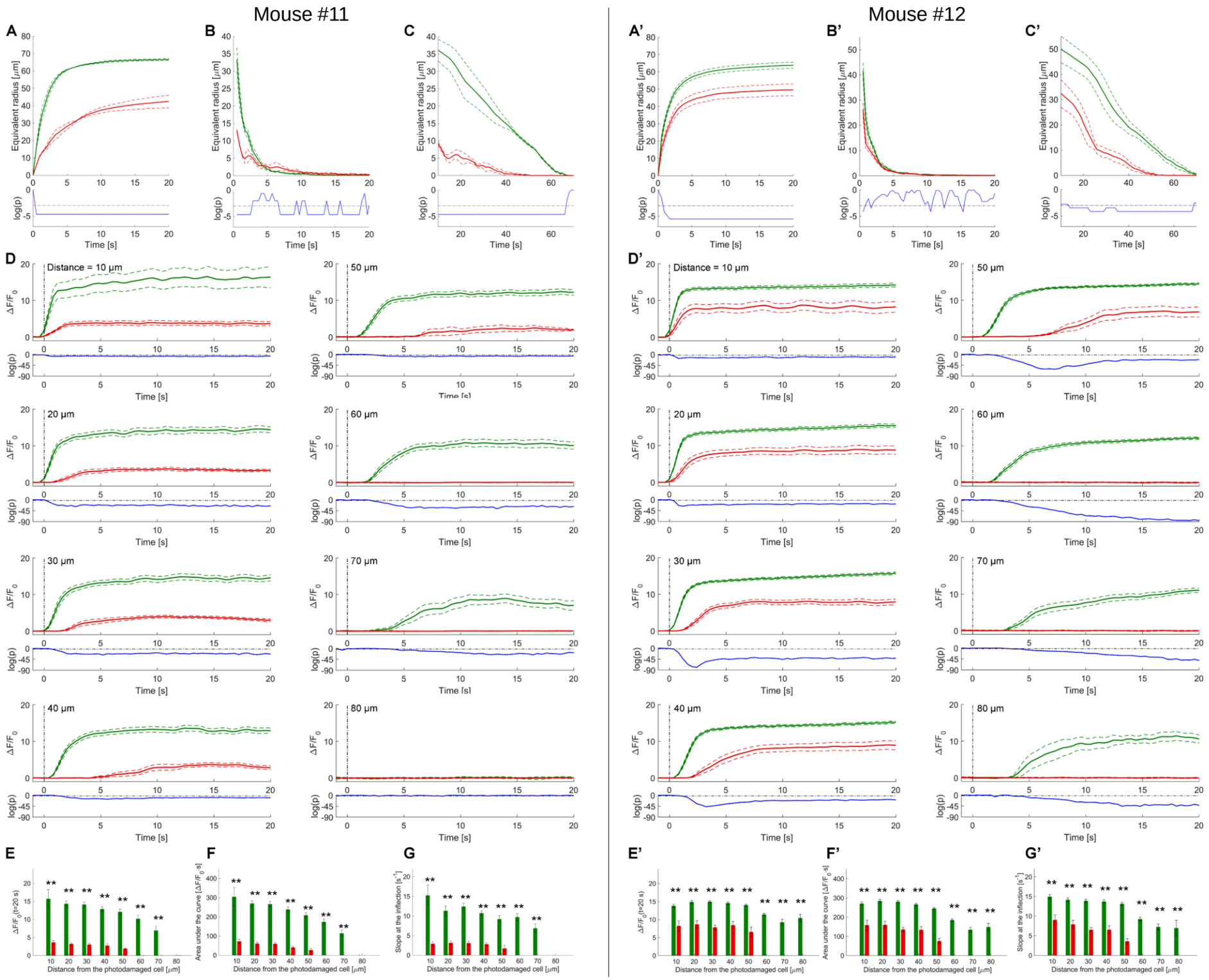

Figure S11: Effect of thapsigargin. (**A**) Equivalent radius of the area invaded by Ca^{2+} waves as a function of time after photodamage; speed of the expanding wave as function of time (**B**) and of the equivalent radius (**C**). (**D**) $\Delta F(t)/F_0$ responses of bystander keratinocytes at increasing distance from the photodamage site. In each panel, the vertical black dash-dotted line at 0 s marks the end of the 0.5 s photodamage time interval. Data in (**A-D**) are mean (solid line) ± s.e.m. (dashed line) in control conditions (green) and after thapsigargin (440 nM) microinjection (red). Point-by-point p-values (p; Wilcoxon Rank Sum test for **A-C**; two-sample t-test for **D**) are shown on a logarithmic scale below each graph (blue traces); $p < 0.05$ (horizontal black dash-dotted line) indicates statistical significance. (**E**) Amplitude of the $\Delta F(t)/F_0$ signal at time t=20 s. (**F**) Area (I) under the $\Delta F(t)/F_0$trace, computed between 0 and 20 s. (**G**) Slope (s) of the $\Delta F(t)/F_0$ trace at the inflection point. Data in (**E-G**) are mean ± s.e.m. vs. bystander cell distance from the photodamage site in control conditions (green) and after thapsigargin microinjection (red). Experiments in **A-G** were conducted in n=3 (control) and n=3 (thapsigargin) non-overlapping areas of the mouse earlobe skin. P-values differences in **E-G** are shown above each pair of bars (two-sample t-test): *=p-value<0.05; **=p-value<0.005. (**A'-G'**) The same experiments were repeated on a different mouse, in n=5 (control) and n=4 (thapsigargin) non-overlapping areas of earlobe skin.

Carbenoxolone

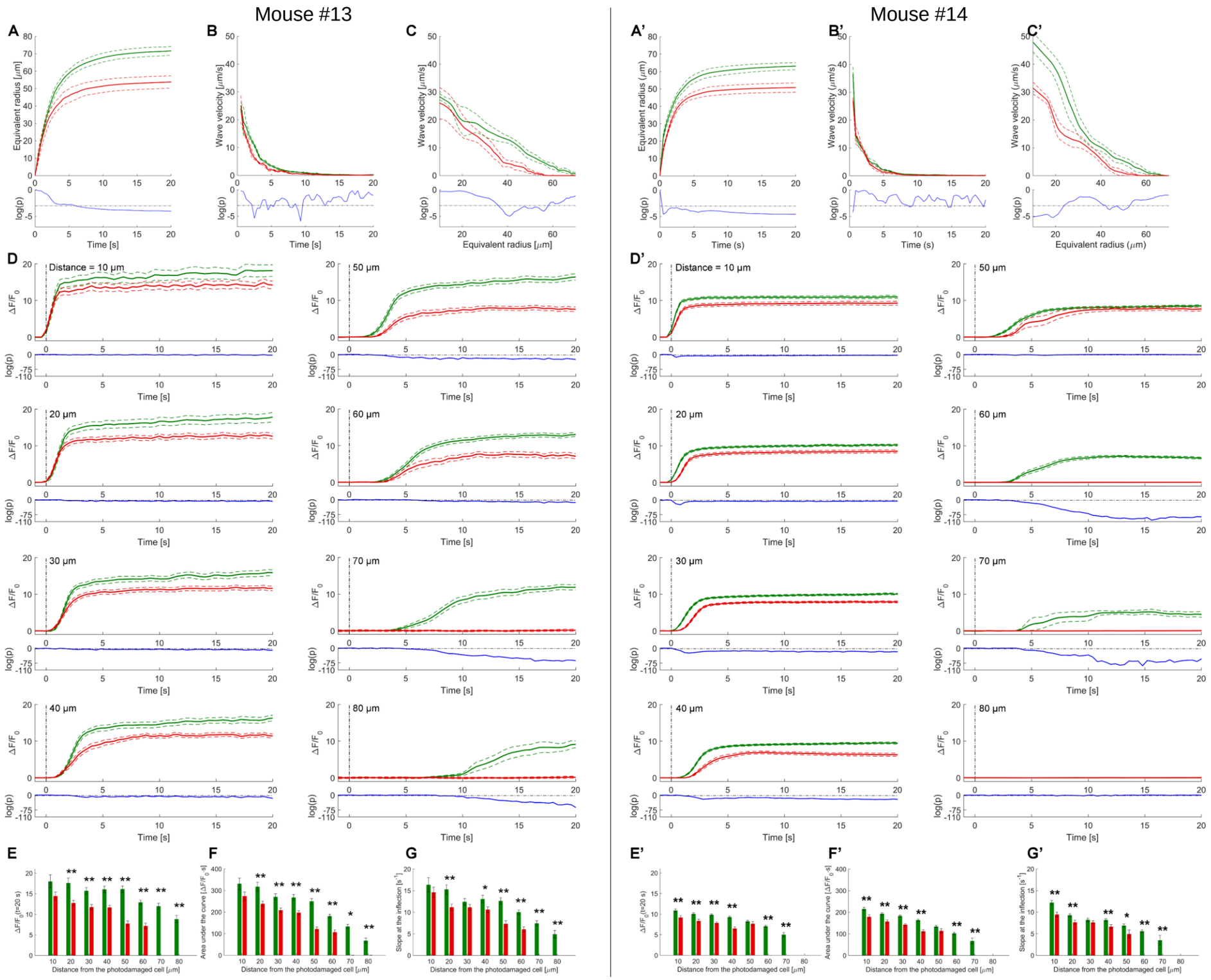

Figure S12: Effect of carbenoxolone (CBX). (**A**) Equivalent radius of the area invaded by Ca^{2+} waves as a function of time after photodamage; speed of the expanding wave as function of time (**B**) and of the equivalent radius (**C**). (**D**) $\Delta F(t)/F_0$ responses of bystander keratinocytes at increasing distance from the photodamage site. In each panel, the vertical black dash-dotted line at 0 s marks the end of the 0.5 s photodamage time interval. Data in (**A-D**) are mean (solid line) ± s.e.m. (dashed line) in control conditions (green) and after CBX (400 µM) microinjection (red). Point-by-point p-values (p; Wilcoxon Rank Sum test for **A-C**; two-sample t-test for **D**) are shown on a logarithmic scale below each graph (blue traces); $p < 0.05$ (horizontal black dash-dotted line) indicates statistical significance. (**E**) Amplitude of the $\Delta F(t)/F_0$ signal at time t=20 s. (**F**) Area (I) under the $\Delta F(t)/F_0$trace, computed between 0 and 20 s. (**G**) Slope (s) of the $\Delta F(t)/F_0$ trace at the inflection point. Data in (**E-G**) are mean ± s.e.m. vs. bystander cell distance from the photodamage site in control conditions (green) and after CBX microinjection (red). Experiments in **A-G** were conducted in n=3 (control) and n=3 (CBX) non-overlapping areas of the mouse earlobe skin. P-values differences in **E-G** are shown above each pair of bars (two-sample t-test): *=p-value<0.05; **=p-value<0.005. (**A'-G'**) The same experiments were repeated on a different mouse, in n=5 (control) and n=4 (CBX) non-overlapping areas of earlobe skin.

Probenecid

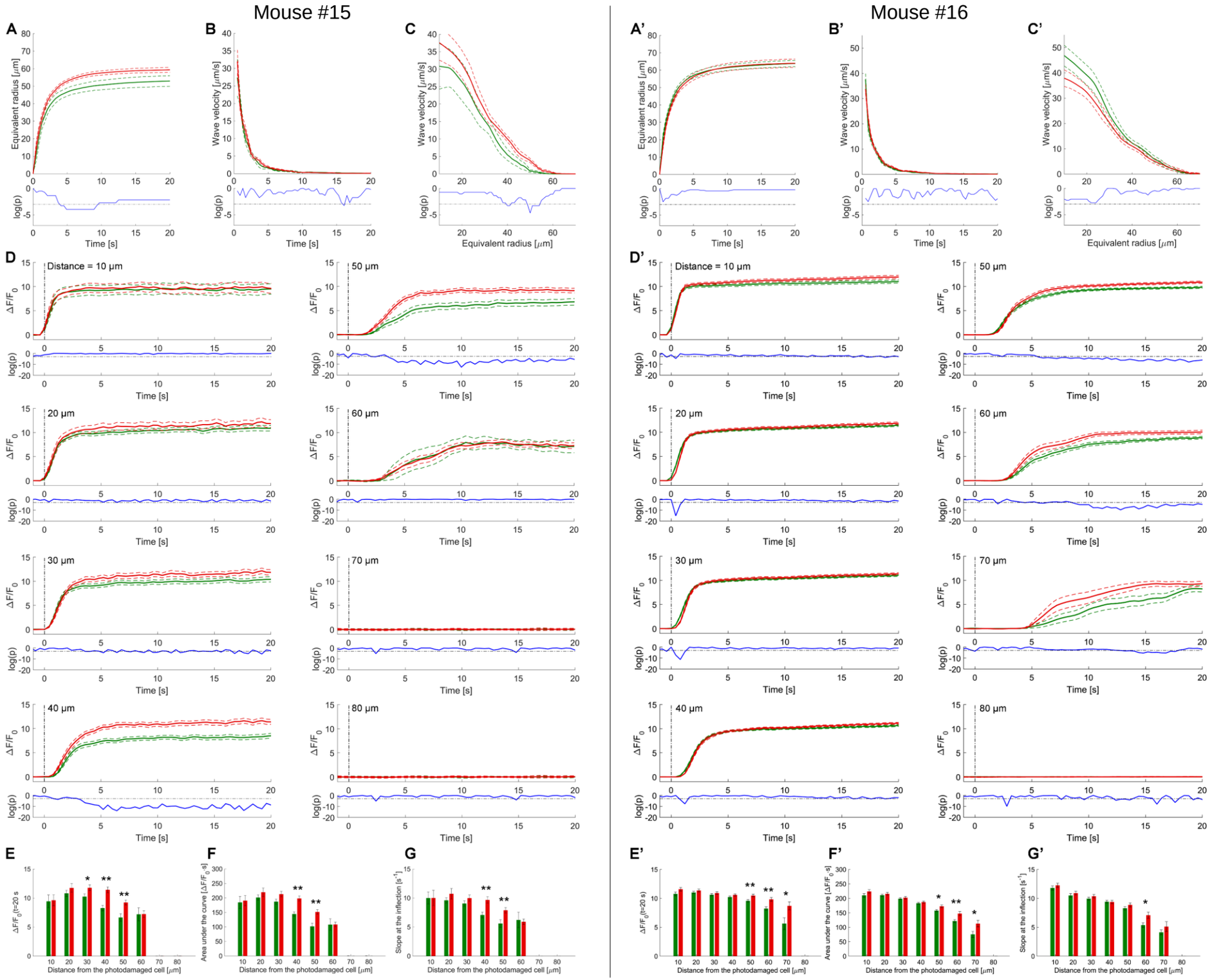

Figure S13: Effect of probenecid. (**A**) Equivalent radius of the area invaded by Ca^{2+} waves as a function of time after photodamage; speed of the expanding wave as function of time (**B**) and of the equivalent radius (**C**). (**D**) $\Delta F(t)/F_0$ responses of bystander keratinocytes at increasing distance from the photodamage site. In each panel, the vertical black dash-dotted line at 0 s marks the end of the 0.5 s photodamage time interval. Data in (**A-D**) are mean (solid line) ± s.e.m. (dashed line) in control conditions (green) and after probenecid (4 mM) microinjection (red). Point-by-point p-values (p; Wilcoxon Rank Sum test for **A-C**; two-sample t-test for **D**) are shown on a logarithmic scale below each graph (blue traces); $p < 0.05$ (horizontal black dash-dotted line) indicates statistical significance. (**E**) Amplitude of the $\Delta F(t)/F_0$ signal at time t=20 s. (**F**) Area (I) under the $\Delta F(t)/F_0$trace, computed between 0 and 20 s. (**G**) Slope (s) of the $\Delta F(t)/F_0$ trace at the inflection point. Data in (**E-G**) are mean ± s.e.m. vs. bystander cell distance from the photodamage site in control conditions (green) and after probenecid microinjection (red). Experiments in **A-G** were conducted in n=4 (control) and n=6 (probenecid) non-overlapping areas of the mouse earlobe skin. P-values differences in **E-G** are shown above each pair of bars (two-sample t-test): *=p-value<0.05; **=p-value<0.005. (**A'-G'**) The same experiments were repeated on a different mouse, in n=8 (control) and n=7 (probenecid) non-overlapping areas of earlobe skin.

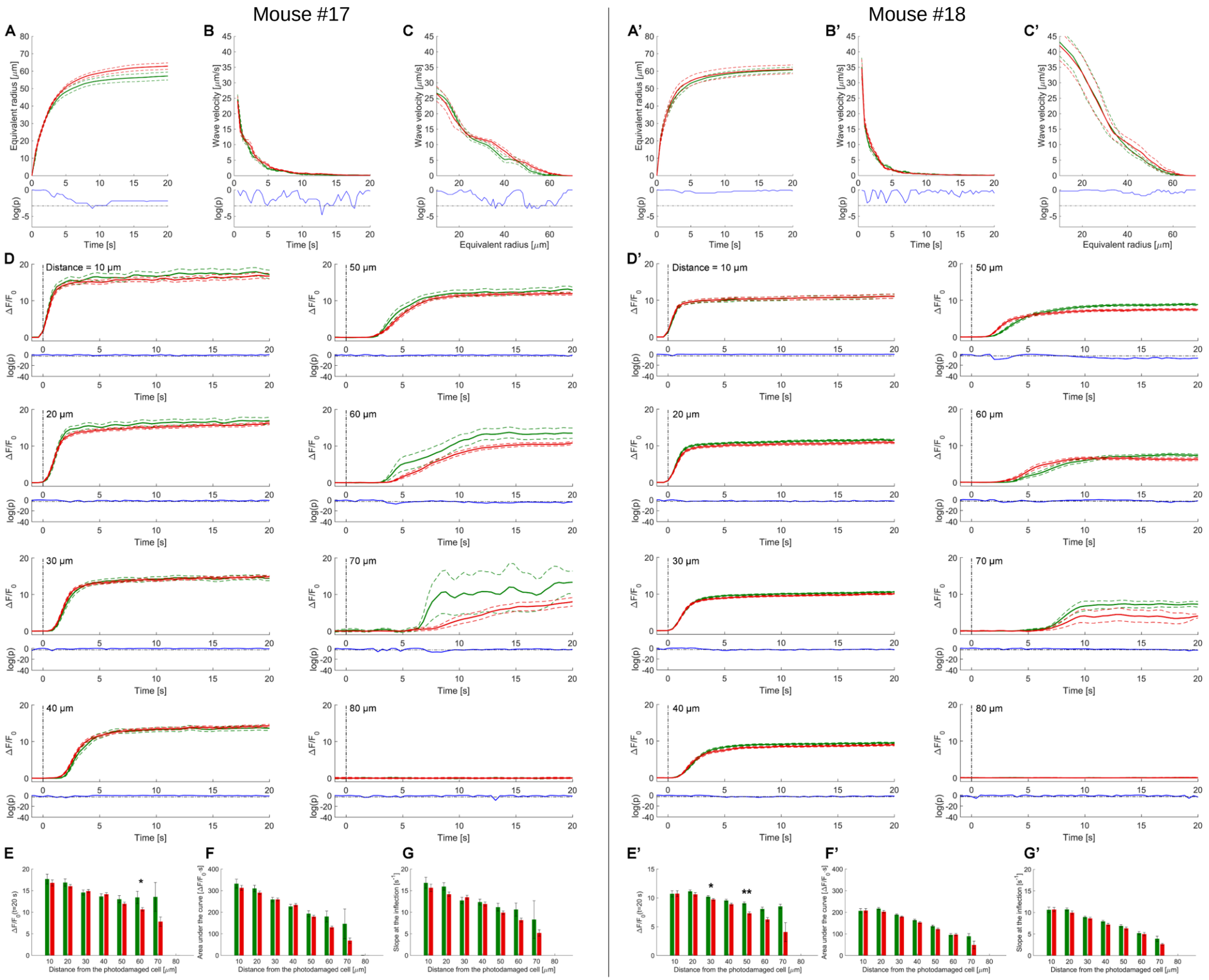

Figure S14: Effect of TAT-gap19. (**A**) Equivalent radius of the area invaded by Ca^{2+} waves as a function of time after photodamage; speed of the expanding wave as function of time (**B**) and of the equivalent radius (**C**). (**D**) $\Delta F(t)/F_0$ responses of bystander keratinocytes at increasing distance from the photodamage site. In each panel, the vertical black dash-dotted line at 0 s marks the end of the 0.5 s photodamage time interval. Data in (**A-D**) are mean (solid line) ± s.e.m. (dashed line) in control conditions (green) and after TAT-gap19 (400 μM) microinjection (red). Point-by-point p-values (p; Wilcoxon Rank Sum test for **A-C**; two-sample t-test for **D**) are shown on a logarithmic scale below each graph (blue traces); $p < 0.05$ (horizontal black dash-dotted line) indicates statistical significance. (**E**) Amplitude of the $\Delta F(t)/F_0$ signal at time t=20 s. (**F**) Area (I) under the $\Delta F(t)/F_0$trace, computed between 0 and 20 s. (**G**) Slope (s) of the $\Delta F(t)/F_0$ trace at the inflection point. Data in (**E-G**) are mean ± s.e.m. vs. bystander cell distance from the photodamage site in control conditions (green) and after TAT-gap19 microinjection (red). Experiments in **A-G** were conducted in n=5 (control) and n=6 (TAT-gap19) non-overlapping areas of the mouse earlobe skin. P-values differences in **E-G** are shown above each pair of bars (two-sample t-test): *=p-value<0.05; **=p-value<0.005. (**A'-G'**) The same experiments were repeated on a different mouse, in n=6 (control) and n=5 (TAT-gap19) non-overlapping areas of earlobe skin.

Table S1: Exact p-values calculated from the comparison between drugs microinjections and their control for the parameter amplitude of the $\Delta F(t)/F_0$ signal at time t=20 s, represented by * above each pair of bars in **Figure 4(i)** and **Figures S6-S14 E**. Two-sample t-test.

		Distance from the photodamaged cell [µm]							
		10	20	30	40	50	60	70	80
Vehicle solution	Mouse 1	0.2	0.4	0.001	0.1	0.3	0.4	0.6	0.6
	Mouse 2	0.9	0.6	0.9	0.4	0.6	0.6	0.6	0.8
Apyrase	Mouse 3	0.04	0.6	4×10^{-32}	2×10^{-26}	1×10^{-19}	3×10^{-11}	2×10^{-21}	0.1
	Mouse 4	0.002	0.02	5×10^{-25}	6×10^{-32}	2×10^{-16}	1×10^{-11}	0.3	0.3
PPADS	Mouse 5	0.05	0.2	0.01	1×10^{-4}	1×10^{-4}	1×10^{-40}	3×10^{-28}	3×10^{-25}
	Mouse 6	9×10^{-7}	1×10^{-11}	8×10^{-14}	4×10^{-14}	3×10^{-10}	7×10^{-46}	1×10^{-24}	0.3
ARL 67156	Mouse 7	1	0.8	0.97	0.8	0.2	0.002	0.9	5×10^{-8}
	Mouse 8	0.2	0.7	0.1	0.7	0.6	3×10^{-5}	2×10^{-38}	3×10^{-24}
EGTA	Mouse 9	7×10^{-5}	5×10^{-8}	2×10^{-9}	1×10^{-11}	1×10^{-8}	1×10^{-5}	0.2	1×10^{-10}
	Mouse 10	1×10^{-16}	5×10^{-25}	1×10^{-26}	7×10^{-33}	8×10^{-42}	1×10^{-33}	2×10^{-15}	1×10^{-26}
Thapsigargin	Mouse 11	3×10^{-4}	1×10^{-12}	6×10^{-12}	7×10^{-6}	2×10^{-4}	4×10^{-13}	5×10^{-10}	0.08
	Mouse 12	1×10^{-5}	1×10^{-8}	3×10^{-19}	4×10^{-10}	8×10^{-12}	2×10^{-33}	1×10^{-14}	6×10^{-20}
CBX	Mouse 13	0.06	4×10^{-4}	1×10^{-4}	1×10^{-5}	2×10^{-11}	6×10^{-7}	1×10^{-3}	4×10^{-28}
	Mouse 14	0.005	3×10^{-4}	2×10^{-8}	2×10^{-19}	0.5	2×10^{-43}	4×10^{-37}	0.1
Probenecid	Mouse 15	0.9	0.3	0.03	2×10^{-5}	1×10^{-3}	0.97	0.09	0.09
	Mouse 16	0.07	0.2	0.3	0.2	0.002	5×10^{-4}	0.02	0.4
TAT-gap19	Mouse 17	0.5	0.3	0.6	0.4	0.2	0.01	0.07	0.2
	Mouse 18	0.96	0.07	0.05	0.07	0.001	0.30	0.1	0.4

Table S2: Exact p-values calculated from the comparison between drugs microinjections and their control for the parameter area (I) under the $\Delta F(t)/F_0$trace, represented by * above each pair of bars in **Figure 4(ii)** and **Figures S6-S14 F**. Two-sample t-test.

		Distance from the photodamaged cell [µm]							
		10	20	30	40	50	60	70	80
Vehicle solution	Mouse 1	0.2	0.5	0.01	0.6	0.1	0.5	0.2	0.2
	Mouse 2	0.9	0.5	0.9	0.4	0.5	0.6	0.4	0.1
Apyrase	Mouse 3	0.1	0.5	5×10^{-32}	1×10^{-26}	3×10^{-20}	1×10^{-8}	5×10^{-18}	0.5
	Mouse 4	8×10^{-4}	3×10^{-5}	3×10^{-21}	2×10^{-21}	1×10^{-12}	1×10^{-18}	0.2	0.2
PPADS	Mouse 5	0.005	0.02	6×10^{-4}	6×10^{-6}	1×10^{-5}	7×10^{-39}	1×10^{-25}	1×10^{-20}
	Mouse 6	2×10^{-7}	1×10^{-13}	4×10^{-18}	3×10^{-19}	3×10^{-15}	7×10^{-43}	3×10^{-20}	0.9
ARL 67156	Mouse 7	0.99	0.8	0.8	0.4	0.004	3×10^{-5}	0.1	3×10^{-5}
	Mouse 8	0.3	0.8	0.08	0.9	0.3	2×10^{-5}	5×10^{-36}	2×10^{-25}
EGTA	Mouse 9	8×10^{-5}	2×10^{-8}	2×10^{-11}	1×10^{-14}	1×10^{-9}	1×10^{-6}	0.8	2×10^{-11}
	Mouse 10	6×10^{-17}	2×10^{-24}	4×10^{-25}	2×10^{-30}	9×10^{-26}	1×10^{-26}	7×10^{-10}	4×10^{-25}
Thapsigargin	Mouse 11	2×10^{-4}	4×10^{-12}	3×10^{-11}	2×10^{-6}	2×10^{-4}	3×10^{-15}	7×10^{-11}	0.7
	Mouse 12	3×10^{-6}	2×10^{-9}	1×10^{-22}	8×10^{-13}	4×10^{-17}	5×10^{-29}	5×10^{-14}	4×10^{-16}
CBX	Mouse 13	0.1	9×10^{-4}	4×10^{-4}	7×10^{-5}	2×10^{-10}	2×10^{-5}	0.01	6×10^{-19}
	Mouse 14	0,002	9×10^{-5}	2×10^{-9}	4×10^{-10}	0.2	1×10^{-35}	1×10^{-25}	0.2
Probenecid	Mouse 15	0.8	0.3	0.05	2×10^{-5}	2×10^{-4}	0.98	0.06	0.06
	Mouse 16	0.1	0.4	0.5	0.4	0.009	0.003	0.03	0.2
TAT-gap19	Mouse 17	0.4	0.2	0.9	0.6	0.3	6×10^{-3}	0.06	0.1
	Mouse 18	0.9	0.07	0.07	0.09	0.05	0.9	0.1	0.1

Table S3: Exact p-values calculated from the comparison between drugs microinjections and their control for the parameter slope (s) of the $\Delta F(t)/F_0$ trace at the inflection point, represented by * above each pair of bars in **Figure 4(iii)** and **Figures S6-S14 G**. Two-sample t-test.

		Distance from the photodamaged cell [µm]							
		10	20	30	40	50	60	70	80
Vehicle solution	Mouse 1	0.2	0.2	0.02	0.9	0.4	0.1	0.99	0.99
	Mouse 2	0.2	0.2	0.1	0.007	0.02	0.5	0.5	0.2
Apyrase	Mouse 3	0.9	0.5	1×10^{-21}	4×10^{-21}	1×10^{-18}	6×10^{-14}	5×10^{-13}	0.5
	Mouse 4	1×10^{-4}	0,002	4×10^{-18}	1×10^{-18}	7×10^{-12}	8×10^{-10}	0.4	0.4
PPADS	Mouse 5	4×10^{-6}	1×10^{-5}	0.07	0.006	0.001	3×10^{-28}	5×10^{-21}	2×10^{-19}
	Mouse 6	4×10^{-11}	6×10^{-11}	8×10^{-11}	9×10^{-12}	5×10^{-12}	2×10^{-32}	1×10^{-18}	0.1
ARL 67156	Mouse 7	0.99	0.8	0.2	0.9	0.04	0.02	0.8	3×10^{-6}
	Mouse 8	0.8	0.2	0.6	0.03	0.4	0.04	5×10^{-27}	1×10^{-25}
EGTA	Mouse 9	0.007	2×10^{-6}	4×10^{-9}	9×10^{-10}	1×10^{-4}	0.004	0.8	4×10^{-25}
	Mouse 10	2×10^{-13}	4×10^{-20}	2×10^{-20}	5×10^{-18}	9×10^{-19}	4×10^{-12}	1×10^{-4}	6×10^{-18}
Thapsigargin	Mouse 11	3×10^{-4}	4×10^{-6}	1×10^{-7}	2×10^{-4}	0.02	9×10^{-31}	3×10^{-10}	0.9
	Mouse 12	9×10^{-6}	2×10^{-7}	3×10^{-16}	5×10^{-8}	1×10^{-10}	1×10^{-17}	2×10^{-11}	4×10^{-9}
CBX	Mouse 13	0.4	1×10^{-3}	0.2	0.02	6×10^{-6}	1×10^{-4}	0.1	3×10^{-18}
	Mouse 14	5×10^{-4}	0.006	0.2	0.006	0.06	7×10^{-31}	4×10^{-18}	0.6
Probenecid	Mouse 15	0.99	0.2	0.2	1×10^{-3}	5×10^{-3}	0.8	0.4	0.4
	Mouse 16	0.4	0.4	0.3	0.9	0.2	0.01	0.4	0.4
TAT-gap19	Mouse 17	0.4	0.06	0.4	0.6	0.1	0.03	0.2	0.9
	Mouse 18	0.9	0.1	0.4	0.09	0.21	0.7	0.2	0.02

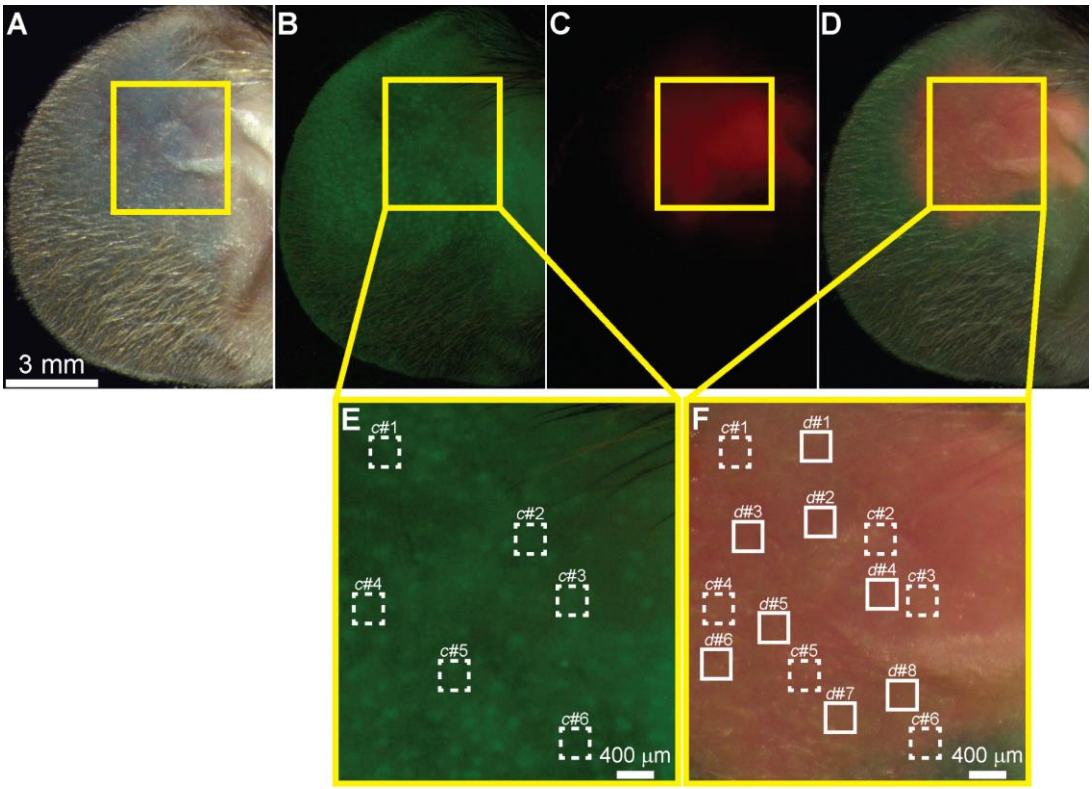

Figure S15: Representative images of a mouse earlobe showing extension of drug-invaded area and non-overlapping fields of view (FOVs) chosen for photodamage (PD) experiments. (**A**) Mouse earlobe reflectance image. (**B**) Green epifluorescence image of GCaMP6s. (**C**) Red epifluorescence image after Dextran, Texas Red injection. (**D**) Merge of **A**, **B**, **C**. (**E**) 3× magnified image of the area contoured by the yellow perimeter in **B**, showing FOVs selected for control (labeled *c#*) PD experiments before drug injection (dashed squares). (**F**) Same as **E**, showing also FOVs selected for PD experiments after injection (solid squares, labeled *d#*). The linear dimension of each FOV area was 317.07 µm.

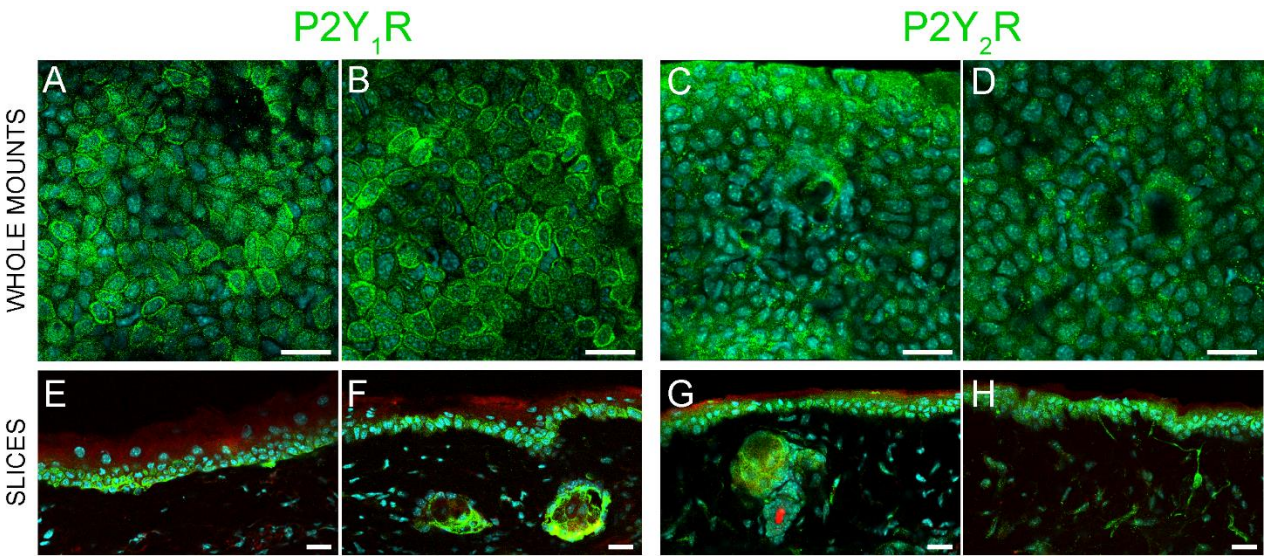

Figure S16: $P2Y_1$ and $P2Y_2$ receptor distributions in the keratinocytes of the basal layer of adult mice epidermis. Representative confocal fluorescence images obtained by immunostaining with antibodies selective for $P2Y_1R$ (**A**, **B**, **E**, **F**) and $P2Y_2R$ (**C**, **D**, **G**, **H**) in whole mount (**A**, **B**, **C**, **D**) and transversal slice (**E**, **F**, **G**, **H**) preparations of adult mice earlobe skin. Cyan: Nuclei stained with 4′,6-Diamidine-2′-phenylindole dihydrochloride (DAPI). Green: P2YR. Only for **E**, **F**, **G**, **H**, red: Skin autofluorescence. Scale bar: 20 μm.

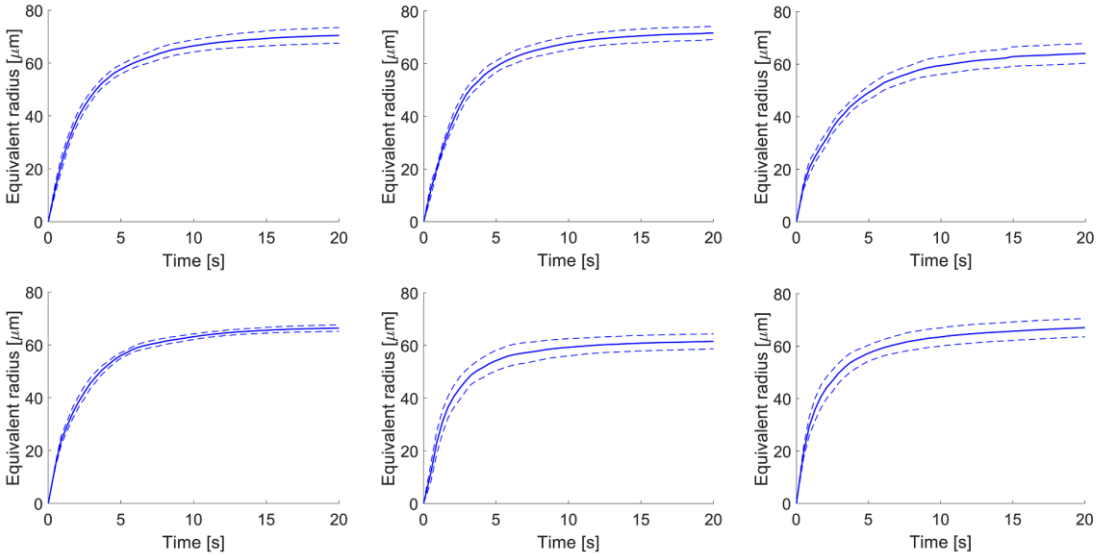

Figure S17: Equivalent radius of the invaded area during Ca^{2+} wave expansion in different anesthetized mice. Mean (blue solid lines) ± s.e.m. (blue dashed lines) of ≥ 3 experiments in each individual mouse (left ordinates).